Electronic Supplementary Material (ESI) for Nanoscale.

Supplementary information

Ultrafast synthesis of SiC nanowire webs by floating catalysts rationalised through in-situ measurements and thermodynamic calculations

Isabel Gómez-Palos,†[a,b] Miguel Vazquez-Pufleau,†[,a] Jorge Valilla,[a,b] Álvaro Ridruejo,[b] Damien Tourret,[a,]*and Juan J. Vilatela[a,]*

[a]IMDEA Materials, Madrid, 28906, Spain. [b]Department of Materials Science, Universidad Politécnica de Madrid, E.T.S. de Ingenieros de Caminos, 28040 Madrid, Spain. [c]Universidad Carlos III de Madrid, 28911 Leganes, Spain. † These authors contributed equally to this work.

*damien.tourret@imdea.org, juanjose.vilatela@imdea.org.

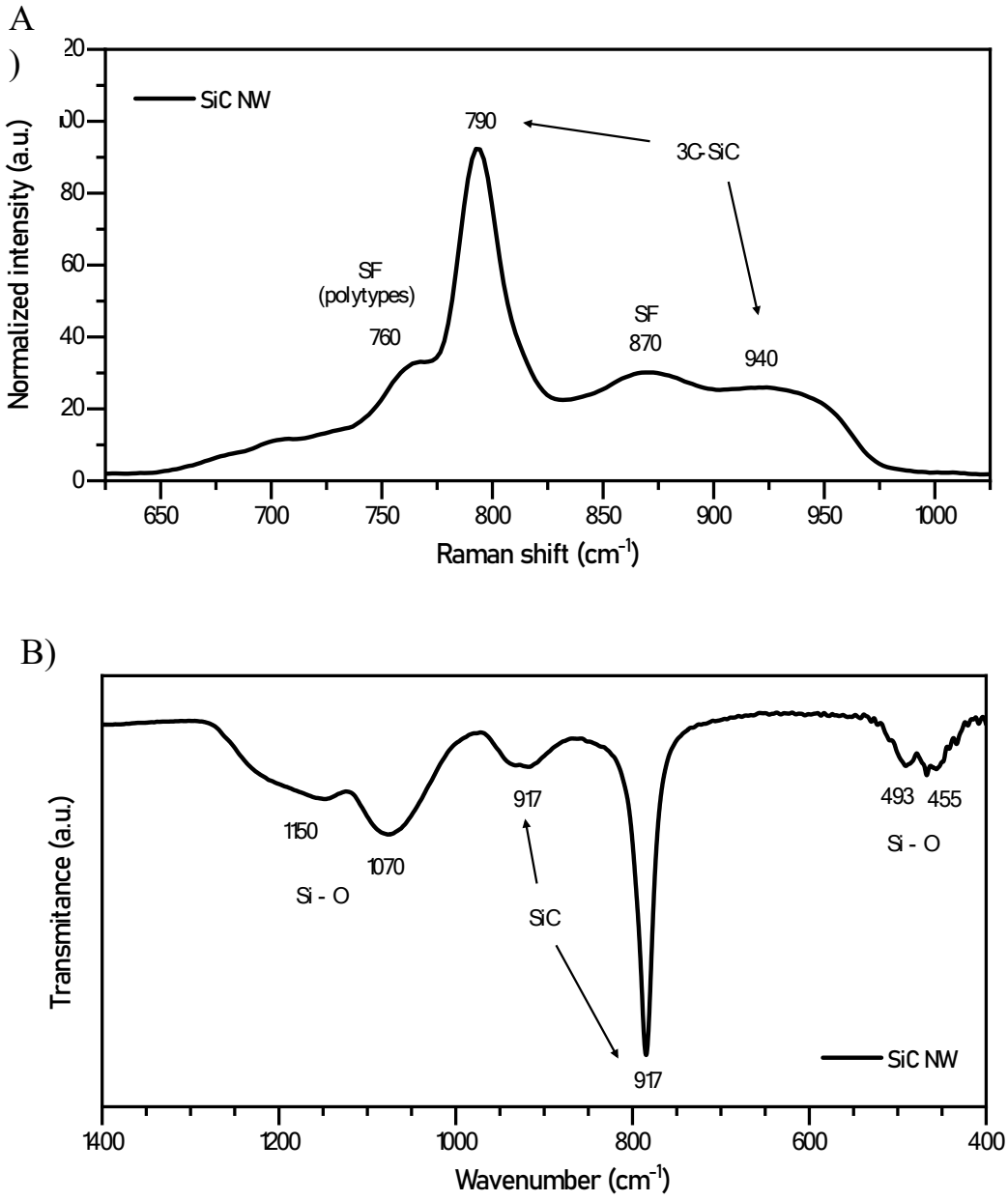

Figure S1 A) Raman shift of SiC nanowires presenting anomalies caused by nanosegments of different polytypes produced during growth because of stacking faults (SF). B) FTIR spectra spectra of freestanding SiC nanowires web.

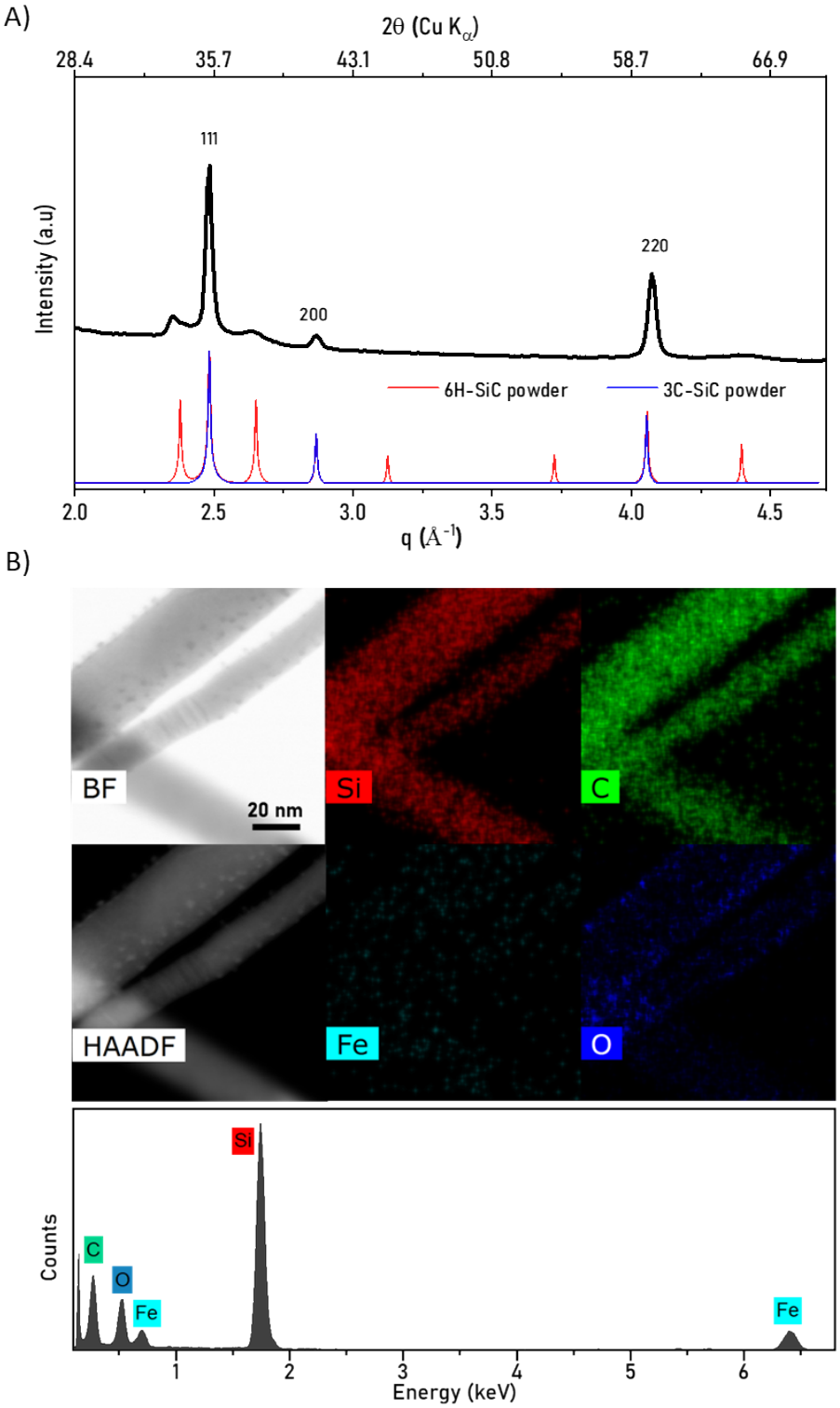

Figure S2 **A)** Synchrotron X-Ray diffraction pattern. Sample (black) compared with the powder spectrum of 6H-SiC (red) and 3C-SiC (blue) phase. **B)** EDX map of SiC nanowires confirming that they are composed of Si and C, with only a thin O shell layer from the native oxide formed from exposure to air. (Fe signal in the spectrum comes from catalyst around the sample)

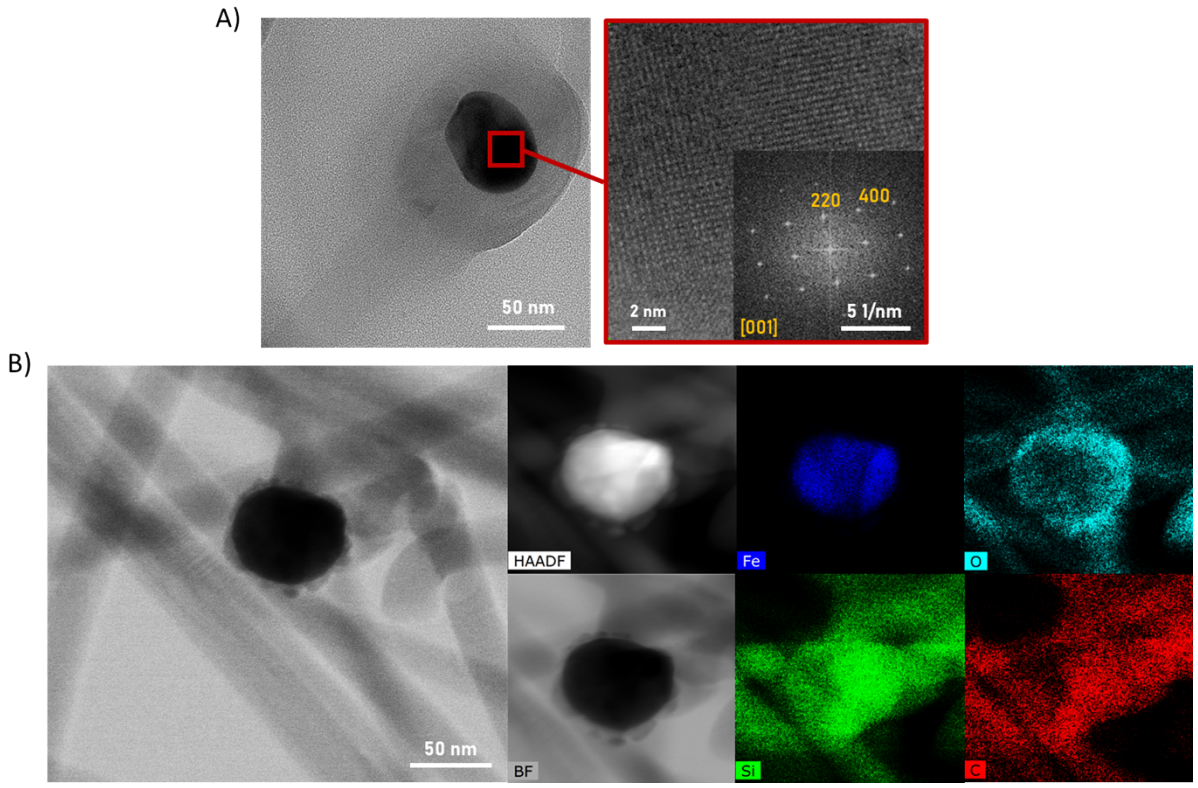

Figure S3. HRTEM images of two different catalyst particles A) FFT showing a lattice spacing of of 0.198 nm (220) and 0.144 nm (400), corresponding to the intermetallic Fe_3Si phase[1] B) Catalyst composition map showing Fe and Si as the conforming elements and a surrounding oxide layer.

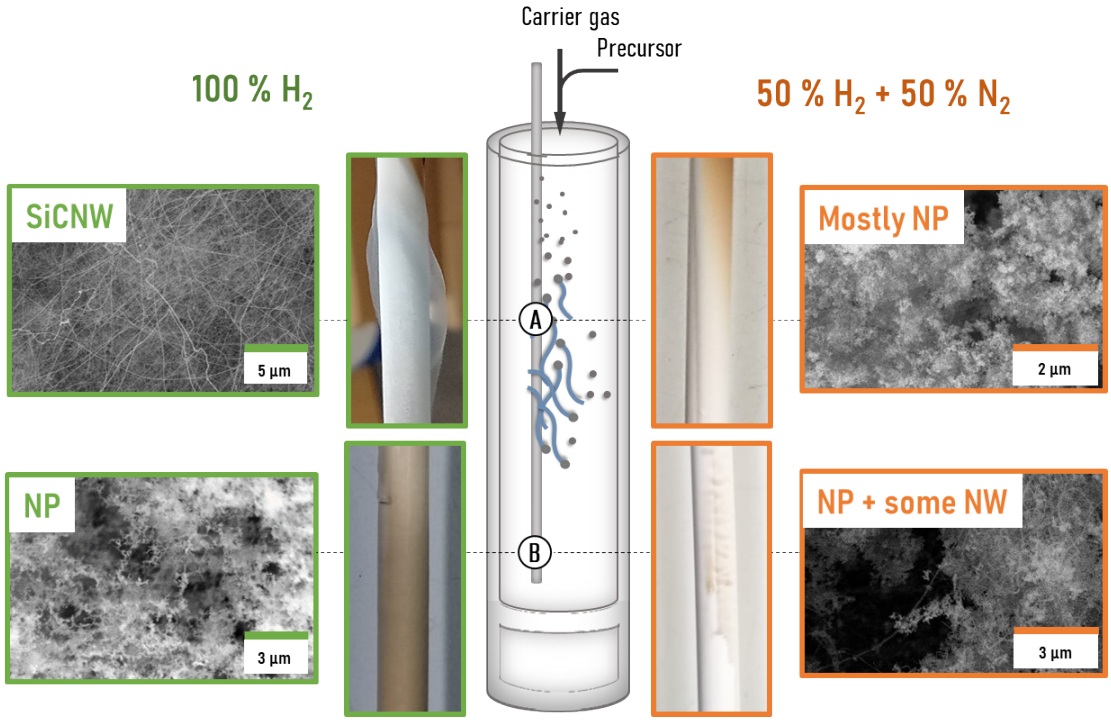

Figure S4 Samples recollected with the mullite rod at 30 cm (position A) and 60 cm (position B) from experiments performed at same conditions but with different concentration of N_2 in the carrier gas, both at total flow of 3 lpm. For pictures highlited in green, pure H_2 was used; while for pictures highlighted in organge, the carrier gas was a mixture 50%/50% of H_2 and N_2.

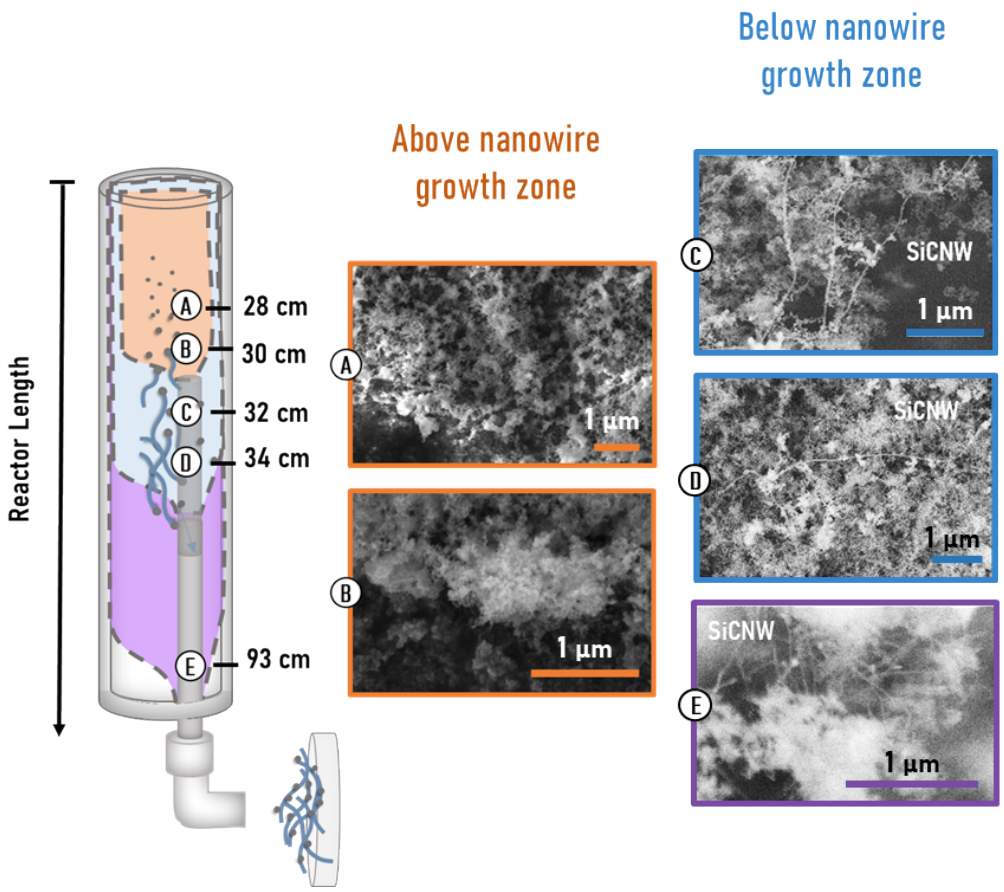

Figure S5 Samples extracted with vacuum collection system at different positions of the reactor, using catalyst produced by ferrocene decomposition. A-B) Samples taken above the nanowire formation zone do not present nanowires, only nanoparticles produced from pyrolysis. C-E) Samples collected in the nanowire zone or bellow present nanowires along with other by-products.

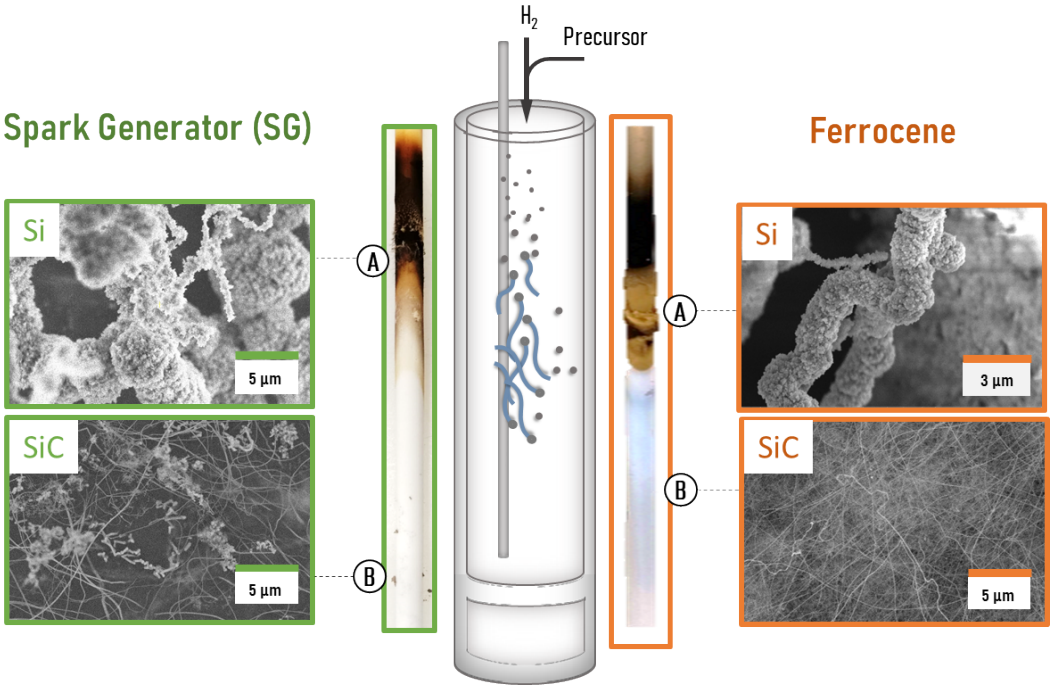

Figure S6 Samples collected from experiments performed at same conditions but different catalyst source, namely, ferrocene and SG. The samples collected with both sources are fairly similar, A) Si microstructures B) SiC NW.

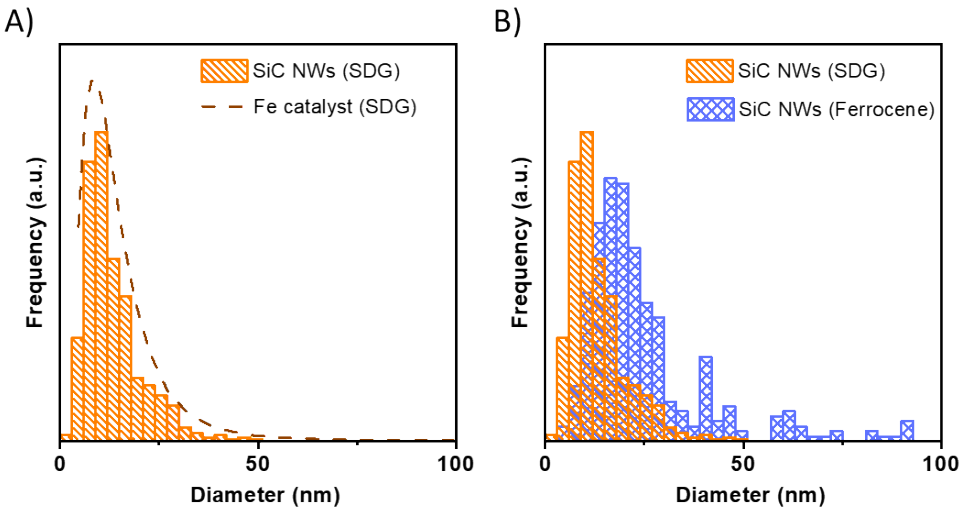

Figure S7. A) Comparison of the diameter distribution of the Fe catalyst produced with SDG (dashed line) obtained with in-situ SMPS analysis at the reaction zone, and the diameter distribution of the nanowires grown with this catalyst source (histogram) obtained from image analysis .The SiC NW diameter matches quite well with the floating SDG Fe catalyst. B) Diameter distribution of NWs grown with different catalyst sources, spark discharge generator (orange) and Ferrocene (blue).

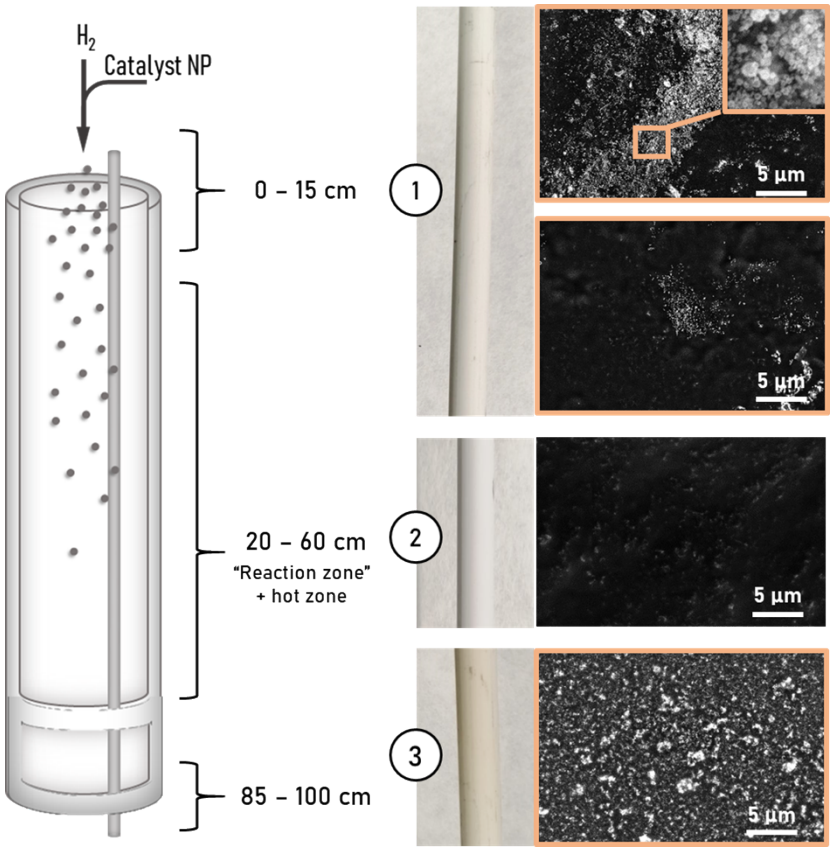

Figure S8. Experiment to probe the possible deposition on the ceramic rod of Fe particles generated with SDG. Particles were only detected at positions 1 and 3, corresponding to temperatures below 600 °C. No evidence of attached particles were found on the section of the ceramic rod at a tempearure corresponding to the "Reaction zone"

Table S1 VLS Growth rate comparison between substrate assisted CVD and this work

Synthesis method	Temp. and carrier gas	Precursors	Catalyst	Special observations	Aspect ratio	Growth time (min)	Growth rate (nm/s)	Reference
CVD	1200 °C, H_2	$SiCl_2$ (g) + Active carbon (s)	Fe	Grown in activated carbon pores	750	90	1.4	Meng 1998 [2]
Hot filament CVD	1000 °C, H_2	Si (s) + graphite (s)	Ni, Cr, Fe impurities	Low pressure	50	120	0.1	Zhou 1999 [3]
Thermal heating (SLS)	1100 °C, Ar	Si substrate (s) + graphite (s)	Ni	WO_3 to reduce graphite	2143	180	6.9	Park 2004 [4]
CVD	1300 °C, Ar	l-PS (l) + Active carbon (s)	Fe	Polymer precursor	66667	180	925.9	Li 2009 [5]
CVD	1150 °C, H_2	HMDS (l)	Ni		500	30	13.9	Panda 2010 [6]
CVD	1500 °C	Si (s) + graphite (s)	Fe		333	360	2.3	Wu 2012 [7]
CVD	1250 °C, H_2	SH4 (g) + CH_4 (g)	Fe		1000	5	166.7	Attolini 2014 [8]
Hot filament CVD	1400 °C, Ar	Si (s) + Active carbon (s)	$LaNi_5$	Catalyst enhancer	375	120	1.0	Rajesh 2014 [9]
CVD	1100 °C, H_2	Si substrate (s) + CH_4 (g)	Fe, Ga, GaN	Catalyst enhancer	12500	45	185.2	Kim 2002 [10]
Thermal heating	1550 °C, Ar	Polysilazane + graphite substrate (s)	Al	low pressure	300	30	16.7	Zhang 2010 [11]
FCCVD	1200 °C, H_2	HMDS (l)	Fe	Floating catalyst- continuous synthesis	1871	0.15	3646	This work

Table S2. Calculated composition of points (a) through (e) in Fig. 6b, in atomic fraction. Point (c) is calculated from thermodynamic equilibrium of Liquid with FCC phase at composition (b), while compositions (b) and (d) are calculated by addition of C and Si from points (a) and (c), respectively, with a C:Si ratio of 1:3 corresponding to HMDS.

	Phase	X(Fe)	X(Si)	X(C)
a	FCC Fe	1.0	0.0	0.0
b	FCC Fe	0.906	0.0235	0.0705
c	Liquid	0.832	0.0202	0.1475
d	Liquid	0.814	0.0248	0.1615
e	Liquid	0.693	0.273	0.034

Length Measurement:

Determining the length of high aspect ratio nanomaterials is established as a long-standing challenge. Despite extensive research on CNTs produced by FCCVD, the only reported estimates of length are a calculation based on the number of ends found in a sample,[12] and indirect measurements using polarised IR spectroscopy.[13] The high aspect ratio of the nanowires in this work makes TEM unsuitable for length measurements. Observation under TEM requires the material to be very thin, essentially as individualised NWs. This implies that they need to be fully dispersed in solvents and then deposited on TEM grids, without shortening them. Previous work on CNTs, SiNWs and now SiCNWs has proven this method unsuccessful. Instead, taking advantage of the relatively large diameter of SiCNWs, we directly image them by high resolution SEM. In this pristine sate though, the NWs are highly entangled, requiring extensive observation to identify NWs with their whole length exposed.

To measure the mean length we used a web collected with the ceramic rod which was then introduced in isopropanol, subjected to mild sonication for 3 minutes. After sonication, a droplet of the material was deposited on top of a flat substrate. Multiple high-resolution images were taken and joined together to create a high quality maps of the nanowire networks, as shown in the example in Figure 3c. Next, the resulting image was visually inspected to identify nanowires whose entire length could be resolved, typically corresponding to those on top of the network and/or near its edges. Their length was determined using Image J. Fig S9 shows an example. This process was applied to five different samples, and a total of 170 nanowires.

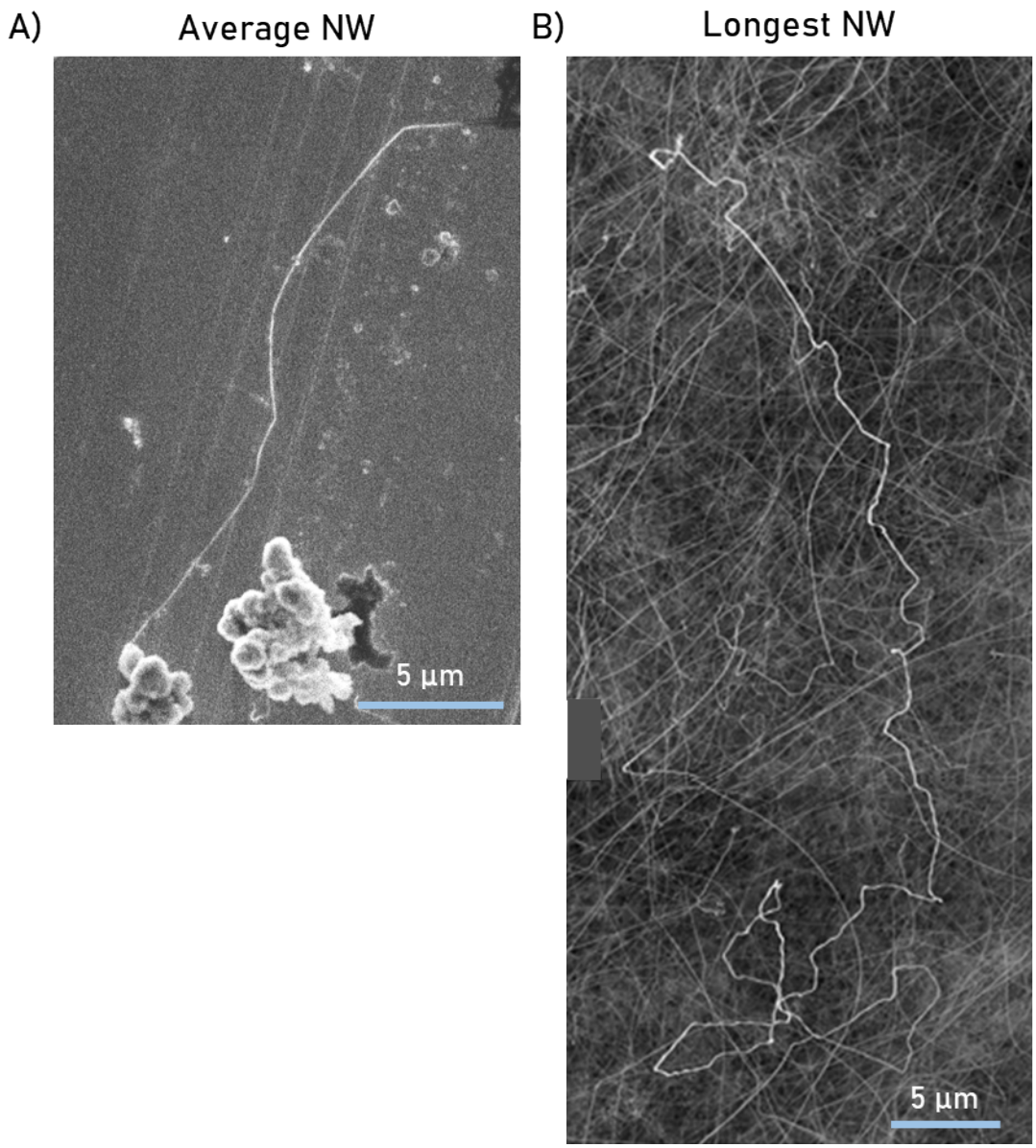

Figure S9. Example of a nanowire with average length and diameter (a) and a SEM micrograph map of the longest nanowire found in sonicated samples synthetised at standard conditions (L = 123 µm, D = 55 nm).

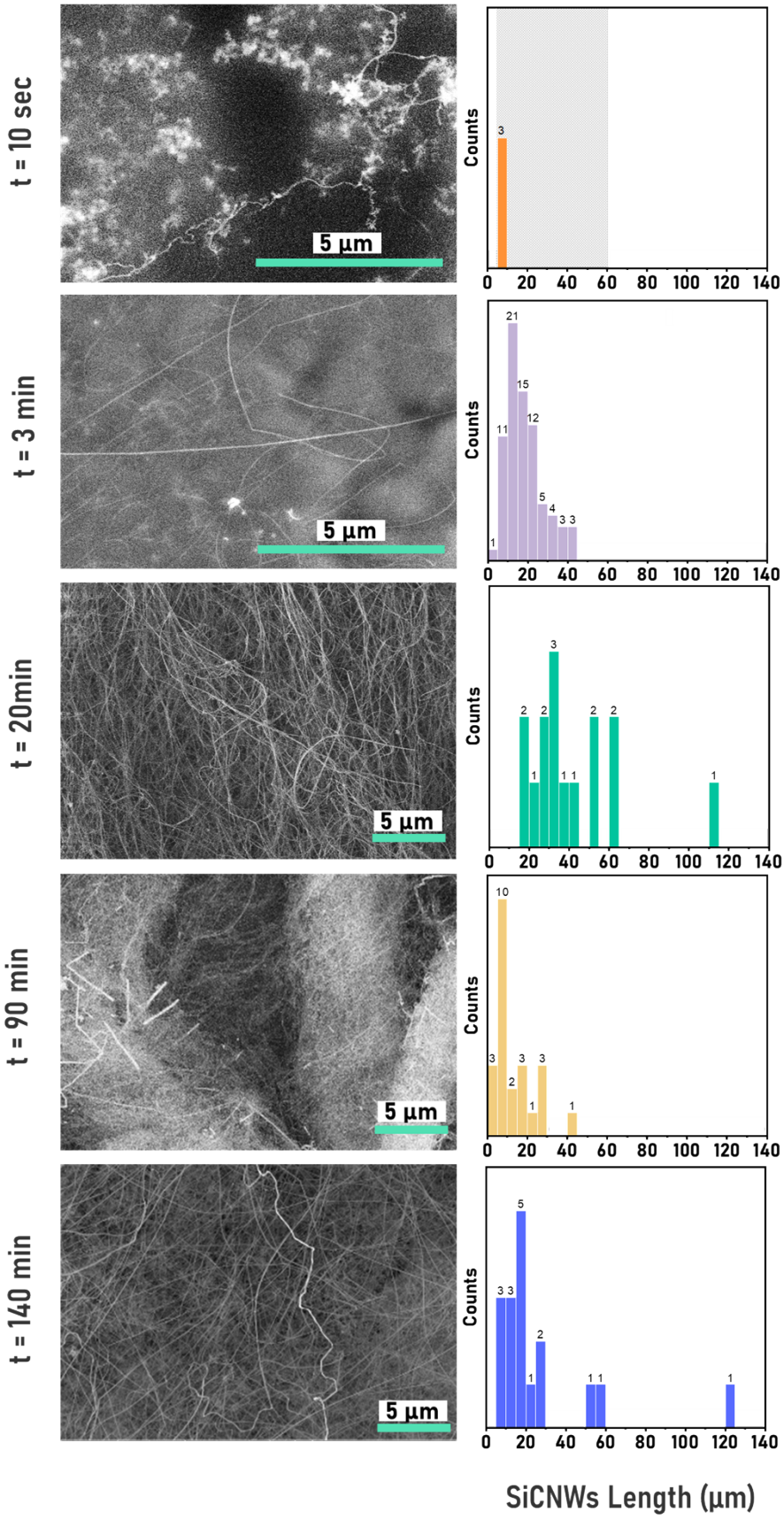

Figure S10. Length of NW collected by the ceramic rod at different experiment times. Standard synthesis conditions were used in all experiments shown.

By-product analysis:

Figure S11 shows examples of high resolution TEM images of the principal solid by-product of the reactor, their FFT confirms the composition as c-Si and amorphous Si-C nanoparticles with some SiC crystalline phases. Examples of samples collected with ceramic rods at different experimental conditions, and the Raman spectra of their different solid products are shown in Figure S12.

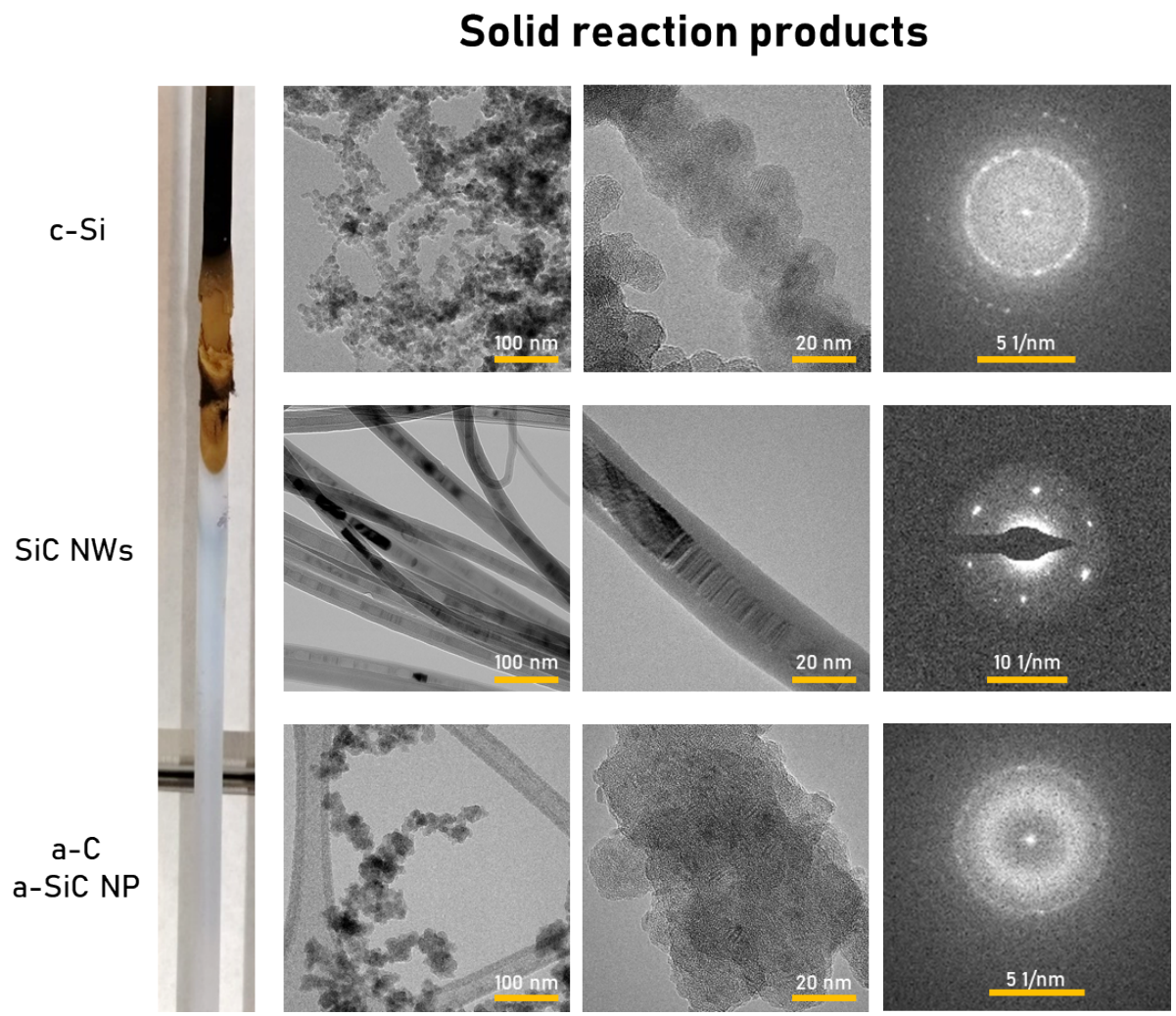

Figure S11. TEM micrographs of the different solids produced at different reaction temperatures and collected on a ceramic rod instered in the reactor tube: Si nanoparticle aggregates, SiC nanowires and SiC/C soot.

Solid reaction products

Variable				
Nominal Temperature	1300 °C	1300 °C	1250 °C	1300 °C
Carrier gas flow	3 lpm	3 lpm	3 lpm	3 lpm
% H2 in carrier gas	100 %	100 %	100 %	90 %
Precursor injection rate	0.5 ml/h	0.5 ml/h	0.5 ml/h	0.5 ml/h
Catalyst Source	Ferrocene	SDG	SDG	SDG

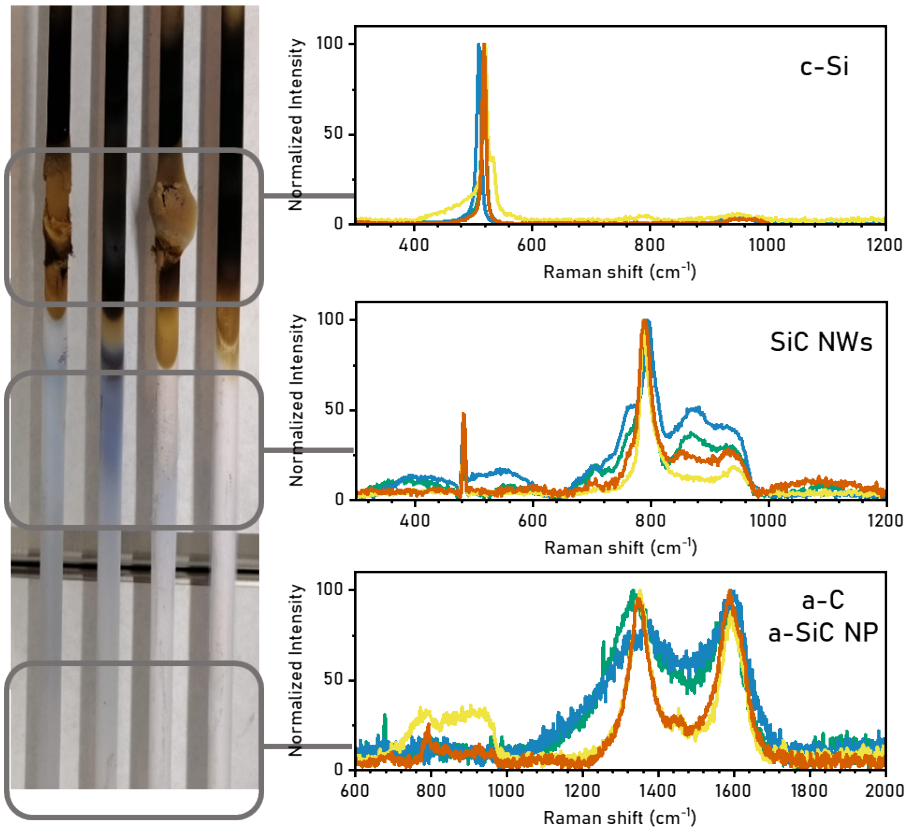

Figure S12. Raman spectra of the different solids produced at different reaction temperatures and collected on a ceramic rod instered in the reactor tube. The composition of the solid products is the same for the range of synthesis conditions studied (Ferroce or SG as catalyst source, 1300 C or 1250 °C, and carrier gas with 10% of nitrogen), although their concentrations may differ.

Sample Collection systems

The ceramic rod and vacuum filter used in this work are expected to have very different collection efficiencies for the different solid particles formed in the reaction. Nanowires, particularly those of high aspect ratio can aggregate, entangle in the gas phase and attach to the surface of the ceramic rod and/or the reactor tube walls. Soot particles are less prone to aggregation and instead more likely

to be collected by the vacuum system. Hence the observation that the material collected on the ceramic cold finger has a higher fraction of NWs than that collected at the cold end of the reactor with the vacuum system. Save for recent work on the formation of carbon nanotube aerogels,[15,16] the dynamics of high aspect ratio nanoparticles floating in a gas stream is a largely unresolved problem.

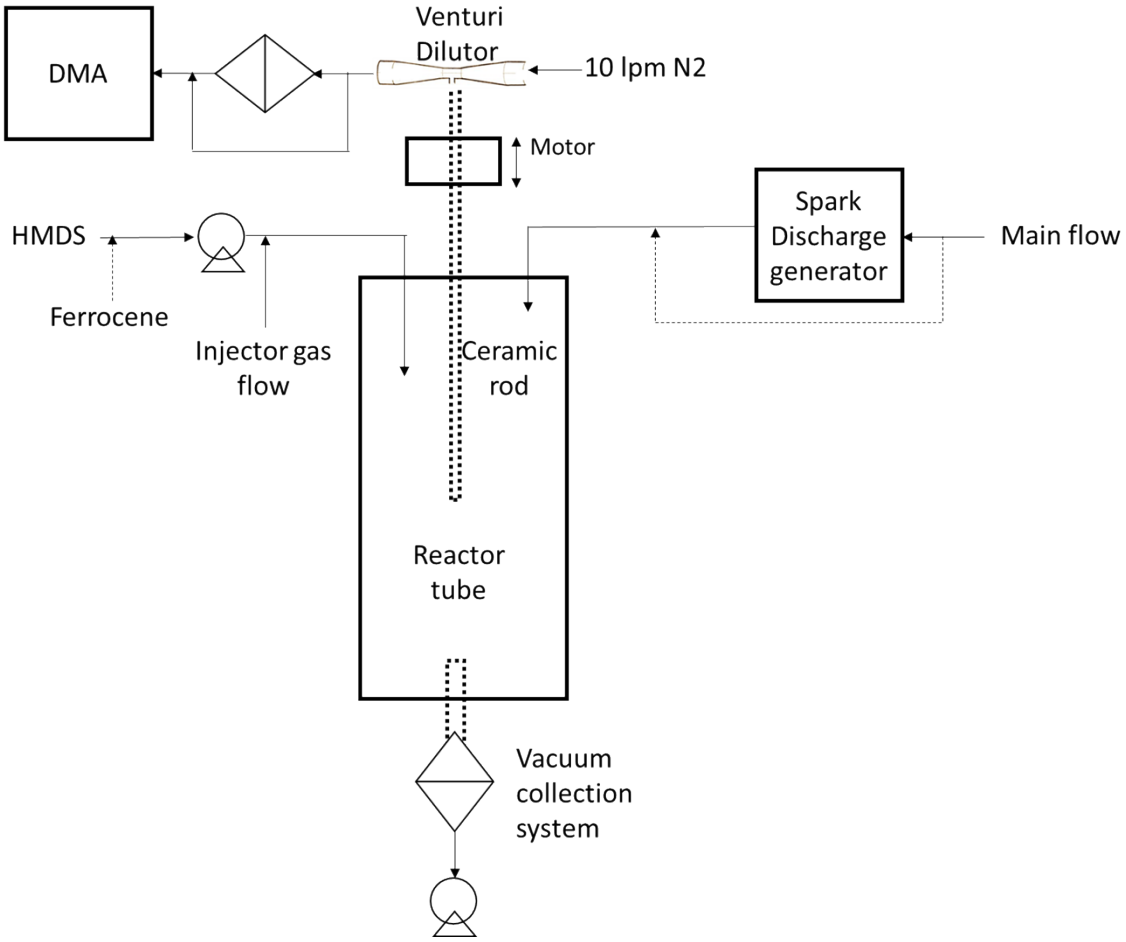

Figure S13. Reactor configuration. Pointed lines represent collection systems that are not used at the same time. Dash lines represent the configuration used when ferrocene is used instead of spark generation to produce the Fe catalyst.

References

1 L. Zhang, H. Zhuang, C. L. Jia and X. Jiang, *CrystEngComm*, 2015, **17**, 7070–7078.

2 G. Meng, L. Zhang, Y. Qin, F. Phillipp, S. Qiao, H. Guo and S. Zhang, *Chinese Phys. Lett.*, 1998, **15**, 689–691.

3 X. T. Zhou, N. Wang, H. L. Lai, H. Y. Peng, I. Bello, N. B. Wong, C. S. Lee and S. T. Lee, *Appl. Phys. Lett.*, 1999, **74**, 3942–3944.

4 B. Park, Y. Ryu and K. Yong, *Surf. Rev. Lett.*, 2004, **11**, 373–378.

5 G. Li, X. Li, Z. Chen, J. Wang, H. Wang and R. Che, *J. Phys. Chem. C*, 2009, **113**, 17655–17660.

6 S. K. Panda, J. Sengupta and C. Jacob, *J. Nanosci. Nanotechnol.*, 2010, **10**, 3046–3052.

7 R. Wu, K. Zhou, J. Wei, Y. Huang, F. Su, J. Chen and L. Wang, *J. Phys. Chem. C*, 2012, **116**, 12940–12945.

8 G. Attolini, F. Rossi, M. Negri, S. C. Dhanabalan, M. Bosi, F. Boschi, P. Lagonegro, P. Lupo and G. Salviati, *Mater. Lett.*, 2014, **124**, 169–172.

9 J. A. Rajesh and A. Pandurangan, *J. Nanosci. Nanotechnol.*, 2014, **14**, 2741–2751.

10 H. Young Kim, J. Park and H. Yang, *Chem. Commun.*, 2003, 256–257.

11 X. Zhang, Y. Chen, Z. Xie and W. Yang, *J. Phys. Chem. C*, 2010, **114**, 8251–8255.

12 M. Motta, A. Moisala, I. A. Kinloch and A. H. Windle, *Adv. Mater.*, , DOI:10.1002/adma.200700516.

13 T. Morimoto, S.-K. Joung, T. Saito, D. N. Futaba, K. Hata and T. Okazaki, *ACS Nano*, 2014, **8**, 9897–9904.

14 H. Liu and P. H. Zwart, *J. Struct. Biol.*, 2012, 180, 226–234.

15 N. Kateris, P. Kloza, R. Qiao, J. A. Elliott and A. M. Boies, *J. Phys. Chem. C*, 2020, **124**, 8359–8370.

16 A. M. Boies, C. Hoecker, A. Bhalerao, N. Kateris, J. de La Verpilliere, B. Graves and F. Smail, *Small*, 2019, **15**, 1900520.